Sensors and Materials, Vol. 36, No. 1 (2024) 37–48
MYU Tokyo

S & M 3496

Flux-vector-controlled Interior Permanent Magnet Synchronous Motor Drive Using Flux Observer Speed Estimation

Yung-Chang Luo,* Zhe-Wei Liao, Hao-You Huang, and Ying-Piao Kuo

Department of Electrical Engineering, National Chin-Yi University of Technology,
No. 57, Sec. 2, Zhongshan Rd, Taiping Dist, Taichung 41170, Taiwan (ROC)

(Received May 26, 2023; accepted December 25, 2023)

Keywords: flux-vector-controlled (FVC) motor drive, interior permanent magnet synchronous motor (IPMSM) drive, speed estimation, flux observer, artificial bee colony (ABC) algorithm

A speed estimation scheme using the flux observer is presented for a flux-vector-controlled (FVC) interior permanent magnet synchronous motor (IPMSM) drive. The decoupled FVC IPMSM drive was established using the current and flux of the stator, and the Hall effect current sensors were used to acquire the three-phase stator current from the IPMSM. The speed estimation scheme based on the flux observer was developed in accordance with Lyapunov stability theory, and the observer gain matrix was designed using the artificial bee colony (ABC) algorithm. MATLAB\Simulink® toolbox was used to simulate this system, and all the control algorithms were realized by a TI DSP 6713-and-F2812 micro-control card to validate this approach. Simulation and experimental results confirmed the effectiveness of the proposed approach.

1. Introduction

Reducing carbon emissions and saving energy are important issues for taking care of the living environment and protecting natural resources. Replacing fuel-powered vehicles with electric vehicles can effectively reduce carbon emissions and significantly reduce energy consumption in transportation. The development of electric vehicles can effectively reduce carbon emissions and greatly lessen energy consumption. The interior permanent magnet synchronous motor (IPMSM) has the advantages of high torque-to-inertia ratio, high power-to-mass ratio, high power factor, high efficiency, and small volume compared with other types of motors, making it a suitable electric vehicle actuation motor. A flux vector control method makes an IPMSM drive similar to a separately excited DC motor drive to realize independent control of torque and flux. According to the flux vector control theory,(1) through coordinate transformation, the three-phase currents of an IPMSM can be distributed into the flux-current and torque-current components, both of which are orthogonal and can be independently controlled to achieve the maximum torque-to-current ratio. The implementation of a traditional flux-vector-controlled (FVC) IPMSM drive requires a position sensor, such as a digital encoder

*Corresponding author: e-mail: luoyc@ncut.edu.tw
https://doi.org/10.18494/SAM4528

ISSN 0914-4935
https://myukk.org/

or an analog resolver, to detect rotor position. However, this sensor reduces the drive robustness and is unsuitable for hostile environments. Therefore, developing a speed estimation FVC IPMSM drive in place of the traditional one is necessary. Some speed detection methods for FVC IPMSM drives are published in the literature: speed prediction by the high frequency signal injection method,[2–5] speed identification based on the back electromotive force (EMF) of the motor,[6–9] speed adaptation by the flux estimator,[10–12] and speed estimation using adaptive control theory.[13–16] In our research, the decoupled FVC IPMSM drive was established using the current and flux of the stator, and the measured stator current signals were obtained from an IPMSM using the electromagnetic Hall effect current sensors. A flux observer speed estimation scheme was developed on the basis of Lyapunov stability theory, and the observer gain matrix was designed using the artificial bee colony (ABC) algorithm. These approaches guaranteed the development of a promising speed estimation FVC IPMSM drive.

This paper comprises six sections. In Sect. 1, we present the research background and motivation, and review the literature on speed estimation methods for FVC IPMSM drives. In Sect. 2, the decoupled FVC IPMSM drive system and linear controller design are described. The details of the design of the flux observer speed estimation scheme on the basis of Lyapunov stability theory are given in Sect. 3. In Sect. 4, we explain the observer gain matrix design using the ABC algorithm in detail. Sections 5 and 6 cover the simulation and experimental results, discussion, and conclusions.

2. Decoupled FVC IPMSM Drive

The two-axis stator current state equations of an IPMSM in the synchronous reference coordinate frame are given by[17]

$$pi_{ds}^{e} = -(R_s / L_d) i_{ds}^{e} + \omega_e (L_q / L_d) i_{qs}^{e} + (1/L_d) v_{ds}^{e}, \tag{1}$$

$$pi_{qs}^{e} = -(R_s / L_q) i_{qs}^{e} - \omega_e (L_d / L_q) i_{ds}^{e} - \omega_e (1/L_q) \lambda_f + (1/L_q) v_{qs}^{e}, \tag{2}$$

where $p = d/dt$ is the differential operator; j stands for the imaginary part; i_{ds}^{e} and i_{qs}^{e}, v_{ds}^{e} and v_{qs}^{e} are the d-axis and q-axis current and voltage of the stator, respectively; L_d and L_q are the d-axis and q-axis stator inductance, respectively; R_s is the stator resistance; λ_f is the equivalent rotor magnet flux produced by the permanent magnet of the rotor; and ω_e is the speed of the synchronous reference coordinate frame.

An examination of Eq. (1) shows that the second term on the right side is a coupling component related to the q-axis stator current. An examination of Eq. (2) reveals that the second and third terms on the right side are the coupling components in relation to the d-axis stator current and rotor magnet flux, respectively. On the basis of these coupling components, the d-axis and q-axis stator voltage feed-forward compensations are defined as

$$v_{ds\_cp}^{e} = -\omega_e (L_q / L_d) i_{qs}^{e}, \tag{3}$$

$$v_{qs\_cp}^{e} = \omega_e (L_d / L_q) i_{ds}^{e} + \omega_e (1/L_q) \lambda_f. \tag{4}$$

Hence, the *d*-axis and *q*-axis linear stator current state equations are decoupled from Eqs. (1) and (2) to Eqs. (5) and (6)

$$p i_{ds}^{e} = -(R_s / L_d) i_{ds}^{e} + (1/L_d) v_{ds}^{e'}, \tag{5}$$

$$p i_{qs}^{e} = -(R_s / L_q) i_{qs}^{e} + (1/L_q) v_{qs}^{e'}, \tag{6}$$

where $v_{ds}^{e'}$ and $v_{qs}^{e'}$ are the outputs of the *d*-axis and *q*-axis stator current controllers, respectively. The voltage commands of the *d*-axis and *q*-axis stator current control loops are expressed as

$$v_{ds}^{e^*} = v_{ds}^{e'} + v_{ds\_cp}^{e}, \tag{7}$$

$$v_{qs}^{e^*} = v_{qs}^{e'} + v_{qs\_cp}^{e}, \tag{8}$$

where $v_{ds}^{e^*}$ and $v_{qs}^{e^*}$ are the voltage commands of the *d*-axis and *q*-axis stator current control loops, respectively. The generated torque of an IPMSM is derived using

$$T_e = (3P/4)(\lambda_f i_{qs}^{e} + (L_d - L_q) i_{qs}^{e} i_{ds}^{e}, \tag{9}$$

where *P* denotes the IPMSM pole numbers. In Eq. (9), the first term on the right side is an electromagnetic torque and the second term is a reluctance torque. The reluctance torque is the additional generated torque of an IPMSM over the surface-mounted permanent magnet synchronous motor. The mechanical equation of the motor is obtained as

$$T_e = J_m p \omega_{rm} + B_m \omega_{rm} + T_L, \tag{10}$$

where J_m and B_m respectively are the motor inertia and the viscous friction coefficient, T_L is the load torque, $\omega_{rm} = (2/P)\omega_r$ is the mechanical speed of the motor rotor shaft, and ω_r is the electric speed of the rotor.

On the basis of Eqs. (5) and (6), the plant transfer functions of the *d*-axis and *q*-axis stator current control loops are respectively derived as

$$G_{p\_i_{ds}}(s) = \frac{1/L_d}{s + R_s/L_d}, \tag{11}$$

$$G_{p\_i_{qs}}(s) = \frac{1/L_q}{s + R_s/L_q}, \tag{12}$$

where s is the Laplace operator. The bandwidth of the inner stator current control loop is much higher than that of the outer speed control loop. In accordance with Eq. (10), the plant transfer function of the speed control loop is given by

$$G_{p\_speed}(s) = \frac{1/J_m}{s + B_m/J_m}. \tag{13}$$

Figure 1 illustrates the decoupled control block diagram of the FVC IPMSM. Here, (K_{ps}, K_{is}), (K_{pd}, K_{id}), and (K_{pd}, K_{pq}) are the proportional and integral gain pairs of the speed controller, and d-axis and q-axis stator current controllers, respectively. Given that the rotor flux is a permanent magnet, the d-axis stator current command is set as a value of 0.

3. Speed Estimation Scheme Based on the Flux Observer

In this research, the feedback speed signal of the conventional FVC IPMSM drive is replaced by an estimation speed. This speed estimation scheme was developed on the basis of the flux observer.

3.1 IPMSM based on symmetric impedance matrix

Owing to the rotor speed of the IPMSM being its synchronous speed (ω_e) and based on a symmetric impedance matrix, Eqs. (1) and (2) can also be rewritten as

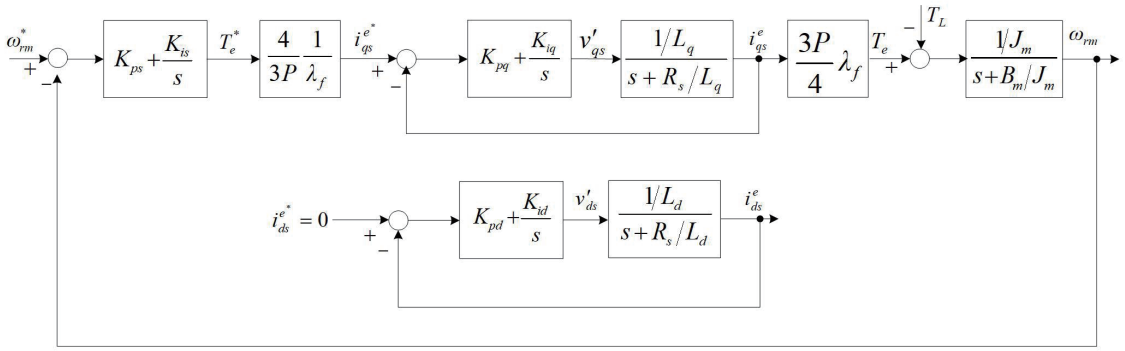

Fig. 1. Block diagram of a decoupling FVC IPMSM drive.

$$\begin{bmatrix} v_{ds}^e \\ v_{qs}^e \end{bmatrix} = \begin{bmatrix} R_s + L_d p & -\omega_r L_q \\ \omega_r L_q & R_s + L_d p \end{bmatrix} \begin{bmatrix} i_{ds}^e \\ i_{qs}^e \end{bmatrix} + \left(\left(L_d - L_q \right) \left(\omega_r i_{ds}^e - p i_{qs}^e \right) + \omega_r \lambda_f \right) \begin{bmatrix} 0 \\ 1 \end{bmatrix}, \tag{14}$$

where $\left(\left(L_d - L_q \right) \left(\omega_r i_{ds}^e - p i_{qs}^e \right) + \omega_r \lambda_f \right)$ is an extended EMF.[18] In the stationary reference coordinate frame, Eq. (14) is given by

$$\begin{bmatrix} v_{ds}^s \\ v_{qs}^s \end{bmatrix} = \begin{bmatrix} R_s + L_d p & -\omega_r (L_d - L_q) \\ \omega_r (L_d - L_q) & R_s + L_d p \end{bmatrix} \begin{bmatrix} i_{ds}^s \\ i_{qs}^s \end{bmatrix} + \left(\left(L_d - L_q \right) \left(\omega_r i_{ds}^s - p i_{qs}^s \right) + \omega_r \lambda_f \right) \begin{bmatrix} -\sin\theta_r \\ \cos\theta_r \end{bmatrix}, \tag{15}$$

where θ_r is the rotor position. In the steady state, the extended EMF is proportional to the rotor speed. Equation (15) can be also rewritten as

$$p \begin{bmatrix} i_{ds}^s \\ i_{qs}^s \end{bmatrix} = \frac{-1}{L_d} \begin{bmatrix} R_s & \omega_r (L_d - L_q) \\ -\omega_r (L_d - L_q) & R_s \end{bmatrix} \begin{bmatrix} i_{ds}^s \\ i_{qs}^s \end{bmatrix} + \frac{1}{L_d} \begin{bmatrix} v_{ds}^s + \omega_r \lambda_{fq}^s \\ v_{qs}^s - \omega_r \lambda_{fd}^s \end{bmatrix}, \tag{16}$$

where λ_{fd}^s and λ_{fq}^s are the *d*-axis and *q*-axis equivalent rotor magnet flux produced by the permanent magnet of the rotor in the stationary reference coordinate frame, respectively.

3.2 Lyapunov stability theory design flux observer

The state matrix of IPMSM expressed by the stator current vector and rotor flux vector in the stationary reference coordinate frame is

$$p \begin{bmatrix} \vec{i}_s^{\,s} \\ \vec{\lambda}_r^{\,s} \end{bmatrix} = \begin{bmatrix} -\frac{R_s}{L_d} - \frac{\omega_r (L_d - L_q)}{L_d} & -\frac{\omega_r}{L_d} \\ 0 & \omega_r \end{bmatrix} \begin{bmatrix} \vec{i}_s^{\,s} \\ \vec{\lambda}_r^{\,s} \end{bmatrix} + \begin{bmatrix} \frac{1}{L_d} \\ 0 \end{bmatrix} \vec{v}_s^{\,s}, \tag{17}$$

where $\vec{i}_s^{\,s} = \begin{bmatrix} i_{ds}^s & i_{qs}^s \end{bmatrix}^T$ is the stator current vector, $\vec{\lambda}_r^{\,s} = \begin{bmatrix} \lambda_{dr}^s & \lambda_{qr}^s \end{bmatrix}^T$ is the rotor flux vector, $\vec{v}_s^{\,s} = \begin{bmatrix} v_{ds}^s & v_{qs}^s \end{bmatrix}^T$ is the stator voltage vector, and $[\bullet]^T$ stands for matrix transpose. In accordance with Eq. (17), the dynamic equations of IPMSM are expressed as[19]

$$\dot{x} = (A + \omega_r A_o) x + Bu, \tag{18}$$

$$y = Cx, \tag{19}$$

where $x = \begin{bmatrix} i_{ds}^s & i_{qs}^s & \lambda_{dr}^s & \lambda_{qr}^s \end{bmatrix}^T$, $A = \begin{bmatrix} -\frac{R_s}{L_d} I & O \\ O & O \end{bmatrix}$, $A_o = \begin{bmatrix} -\frac{L_d - L_q}{L_d} J & -\frac{1}{L_d} J \\ O & J \end{bmatrix}$, $B = \begin{bmatrix} \frac{1}{L_d} I & O \end{bmatrix}^T$, $u = \begin{bmatrix} v_{ds}^s & v_{qs}^s \end{bmatrix}^T$, $C = \begin{bmatrix} I & O \end{bmatrix}$, $I = \begin{bmatrix} 1 & 0 \\ 0 & 1 \end{bmatrix}$, $J = \begin{bmatrix} 0 & -1 \\ 1 & 0 \end{bmatrix}$, and $O = \begin{bmatrix} 0 & 0 \\ 0 & 0 \end{bmatrix}$.

On the basis of Eq. (18), the estimation state equation of IPMSM is derived as

$$\dot{\hat{x}} = (A + \hat{\omega}_r A_o)\hat{x} + Bu + K(\hat{y} - y), \tag{20}$$

where K is a gain matrix. Subtracting Eq. (20) from Eq. (18), the estimation error is given by

$$\dot{e} = (A + \omega_r A_o + KC)e + \Delta\omega_r A_o \hat{x}, \tag{21}$$

where $e = x - \hat{x}$ and $\Delta\omega_r = \omega_r - \hat{\omega}_r$. Define the Lyapunov function as[19]

$$V = (e,\ \Delta\omega_r) = e^T He + \frac{(\Delta\omega_r)^2}{\gamma_\omega}, \tag{22}$$

where H is a symmetric positive definite matrix, and $\gamma_\omega > 0$ is a constant. Then, by differentiating Eq. (22), the time derivative of the Lyapunov function is acquired as

$$\begin{aligned} \dot{V} = {} & e^T[(A + KC)^T H + H(A + KC) + \omega_r(A_o^T H + HA_o)]e \\ & + \Delta\omega_r[\hat{x}^T A_o^T He + e^T HA_o x] - \frac{2\Delta\omega_r}{\gamma_\omega}\frac{d\hat{\omega}_r}{dt}. \end{aligned} \tag{23}$$

In accordance with Lyapunov stability theory,[20] set H and K to confirm that Eq. (24) and inequality Eq. (25) are valid; then Eq. (23) is negative definite.

$$\Delta\omega_r[\hat{x}^T A_o^T He + e^T HA_o x] = (2\Delta\omega_r / \gamma_\omega) \cdot (d\hat{\omega}_r / dt) \tag{24}$$

$$(A + KC)^T H + H(A + KC) + \omega_r(A_o^T H + HA_o) < 0 \tag{25}$$

Hence, Eq. (21) is asymptotically stable, and the established flux observer is also asymptotically stable. On the basis of Eqs. (23), (24), and (25), the adaptive law is selected as

$$\frac{d\hat{\omega}_r}{dt} = e^T HA_o \hat{x}. \tag{26}$$

In accordance with Eq. (26), the estimated rotor speed is derived as

$$\hat{\omega}_r = K_{po}(e^T HA_o\hat{x}) + \frac{1}{s}K_{io}(e^T HA_o x), \tag{27}$$

where K_{po} and K_{io} are the adaptation gains.

The established FVC IPMSM drive using the flux observer speed estimation scheme is displayed in Fig. 2. Here, the speed difference between the rotor speed command (ω_r^*) and estimated rotor speed ($\hat{\omega}_r$) is employed in the FVC IPMSM drive, and via a coordinate transformation, the two-axis synchronous reference frame is transformed to the three-phase stationary reference frame ($2^e \Rightarrow 3^s$) to acquire the three-phase command voltage (v_a, v_b, and v_c) and then to trigger the voltage source inverter to actuate the IPMSM. The stationary coordinate reference frame stator current ($\vec{i}_s^{\,s}$) and voltage ($\vec{v}_s^{\,s}$) are respectively obtained from the synchronous coordinate reference frame stator current ($\vec{i}_s^{\,e}$) and voltage ($\vec{v}_s^{\,e}$) by the coordinate transformation of the two-axis synchronous reference frame to the two-axis stationary reference frame ($2^e \Rightarrow 2^s$). The current difference between the estimated current ($\hat{\vec{i}}_s^{\,s}$) and measured current ($\vec{i}_s^{\,s}$) of the stator is tuned by the observer gain matrix (K) to identify the estimated rotor speed. Moreover, $\vec{i}_s^{\,e}$ is acquired from the IPMSM using the Hall effect current sensors and via the coordinate transformation of the three-phase stationary reference frame to the two-axis synchronous reference frame ($3^s \Rightarrow 2^e$).

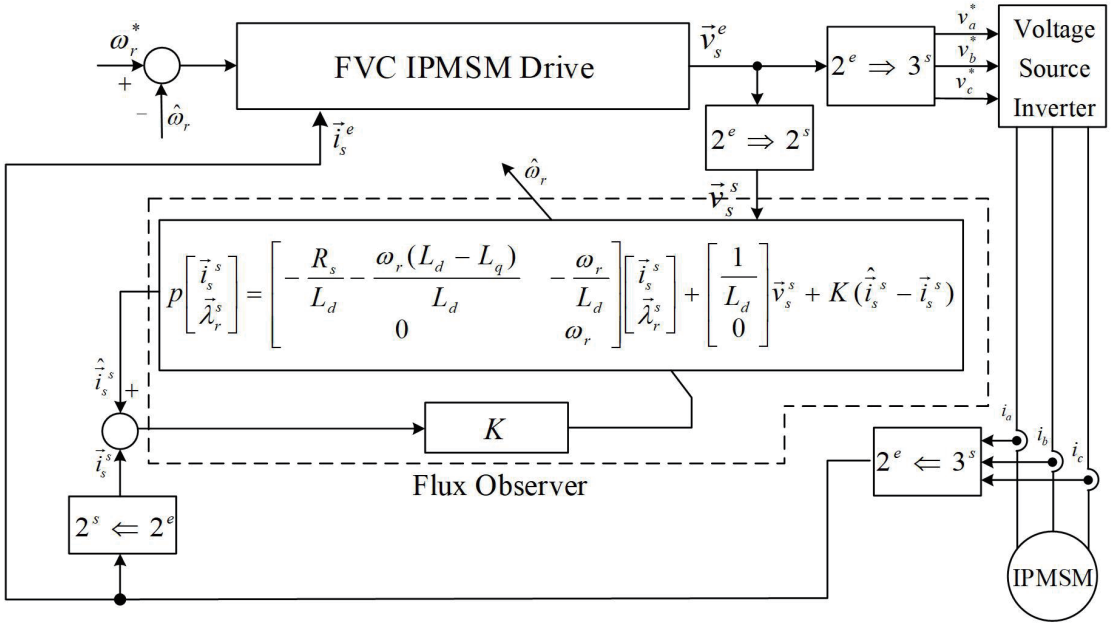

Fig. 2. Speed estimation scheme using the flux observer.

4. Observer Gain Matrix Design Using ABC Algorithm

The ABC algorithm was used to design the observer gain matrix because of its fast convergence, few setting parameters, and a wide search range. The ABC algorithm is one of the swarm intelligence and global optimization algorithms that imitates the behaviors of bee colonies. The ABC algorithm consists of hired, onlooker, and scout bees, which collectively attempt to find the largest nectar source in terms of the amount of nectar.[21] Hired bees are linked to a specific nectar source, and when the nectar source is depleted, hired bees turn into scout bees. Onlooker bees transmit information and select a nectar source on the basis of the information. Scout bees search for nectar sources randomly. During the iterative process, each hired bee searches for the adjacent area of the identified nectar source. Depending on the abundance of the nectar source, using the roulette wheel selection allows the bees to collect nectar. If the nectar source has not changed after several updates, then it is exhausted and discarded. Figure 3 shows the flow chart of the proposed ABC algorithm observer gain matrix design.

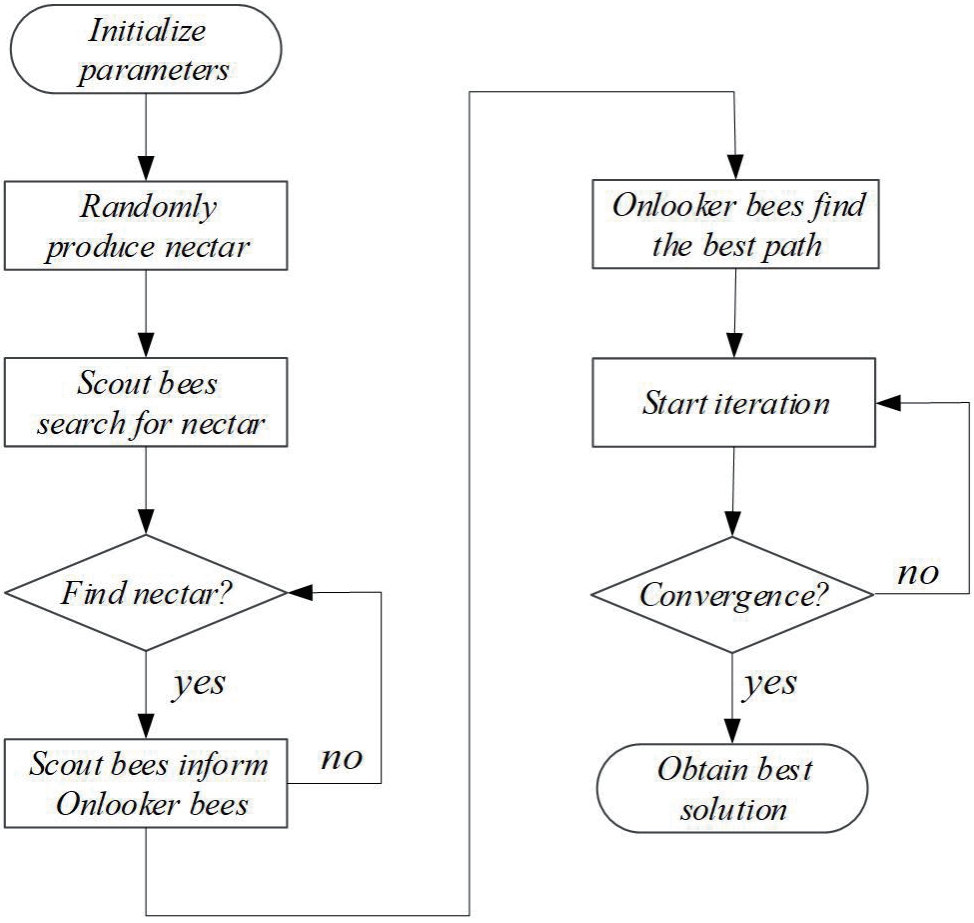

Fig. 3. Flow chart of the proposed ABC algorithm observer gain matrix design.

Figure 4 shows a block diagram of the proposed speed estimation FVC IPMSM drive using the flux observer, which includes a speed controller, *q*-axis and *d*-axis stator current controllers, *d*-axis and *q*-axis stator voltage decoupling, coordinate transformation between the two-axis synchronous reference frame and two-axis stationary reference frame ($2^e \Rightarrow 2^s$, $2^e \Leftarrow 2^s$), coordinate transformation between the three-phase system and two-axis stationary reference frame ($2^s \Rightarrow 3$, $2^s \Leftarrow 3$), and the flux observer speed estimation scheme. In this system, the speed controller and *d*-axis and *q*-axis stator current controllers were designed using the root locus and Bode plot. The observer gain matrix design was used in the ABC algorithm. Furthermore, the three-phase currents (i_{as}, i_{bs}, and i_{cs}) were obtained from the IPMSM using the Hall effect current sensors that completed the coordinate transformation from three-phase reference frame to two-axis stationary reference frame ($2^s \Leftarrow 3$).

5. Simulation Setup and Results

A three-phase, 220 V, 1.5 kW, Y-connected IPMSM serves as the controlled plant for experimentation to confirm the effectiveness of the developed speed estimation FVC IPMSM drive using the flux observer. In a running cycle, the speed command is designed as follows: forward direction acceleration from $t = 0$ to $t = 1$ s, forward direction steady-state running over $1 \le t \le 4$ s, forward direction braking to reach zero speed in the interval $4 \le t \le 5$ s, reverse direction acceleration from $t = 5$ to $t = 6$ s, reverse direction steady-state running over $6 \le t \le 9$ s, and reverse direction braking to reach zero speed in the interval $9 \le t \le 10$ s. Furthermore, in the running cycle, a load of 2 N-m is loaded during $2 \le t \le 3$ s in the forward direction steady state, and $7 \le t \le 8$ s in the reverse direction steady state, respectively.

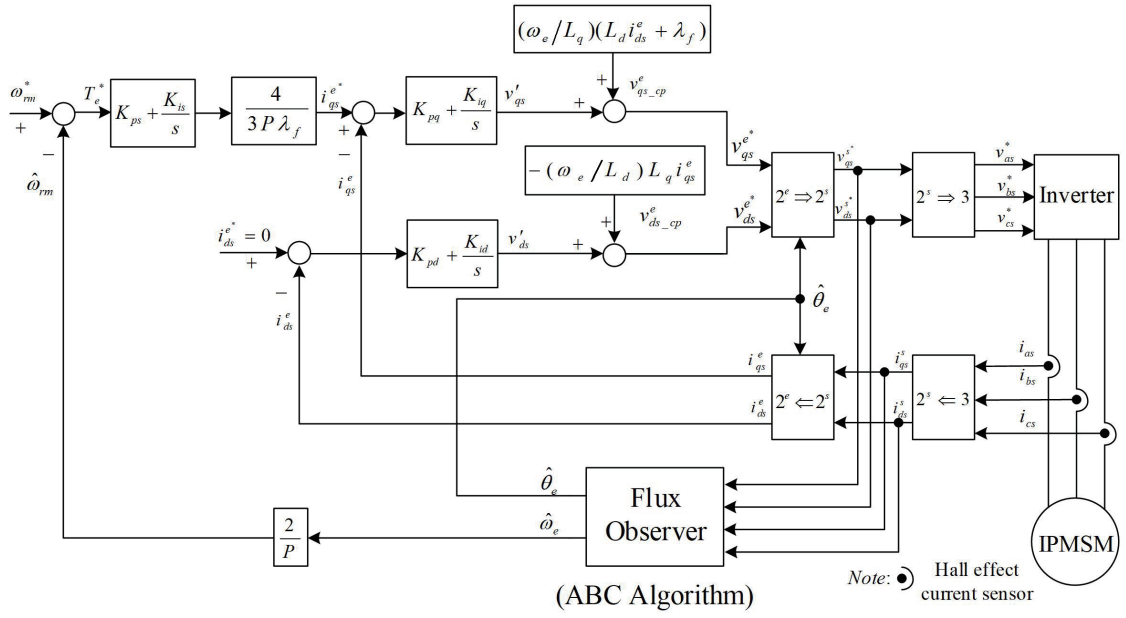

Fig. 4. Speed estimation FVC IPMSM drive using the flux observer.

Figures 5 and 6 present the simulated and measured responses with 2 N-m load for reversible steady-state speed commands at 500 rev/min. Each figure contains six responses: (a) command (dashed line) and estimated (solid line) rotor speed, (b) command (dashed line) and actual (solid) rotor speed, (c) q-axis stator current, (d) electromagnetic torque, (e) flux position angle, and (f) rotor flux locus (q-axis vs d-axis).

According to the simulated and experimental responses, an accurate estimation of rotor speed based on the flux observer was achieved. The circular rotor flux locus and sawtooth flux position angle that confirmed the synchronous position angle (θ_e) can be accurately obtained for implementation in the coordinate transformation between the stationary reference synchronous reference frames. Promising responses for the electromagnetic torque and q-axis stator current, including the reversible transient and steady state, are also effectively realized. Hence, the developed FVC IPMSM drive using the flux observer speed estimation scheme has been shown to have acquired the desired performance.

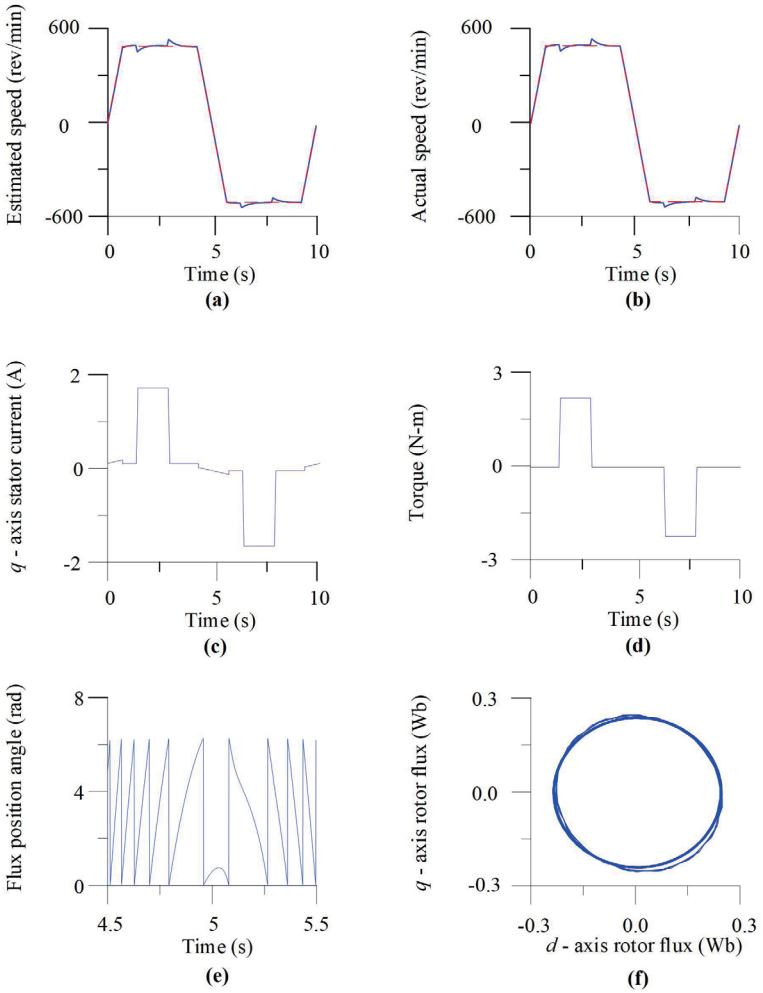

Fig. 5. (Color online) Simulated responses of the proposed FVC IPMSM drive using the flux observer speed estimation with a 2 N-m load for a reversible steady-state speed command of 500 rev/min: (a) estimated rotor speed, (b) actual rotor speed, (c) q-axis stator current, (d) electromagnetic torque, (e) flux position angle, and (f) rotor flux locus.

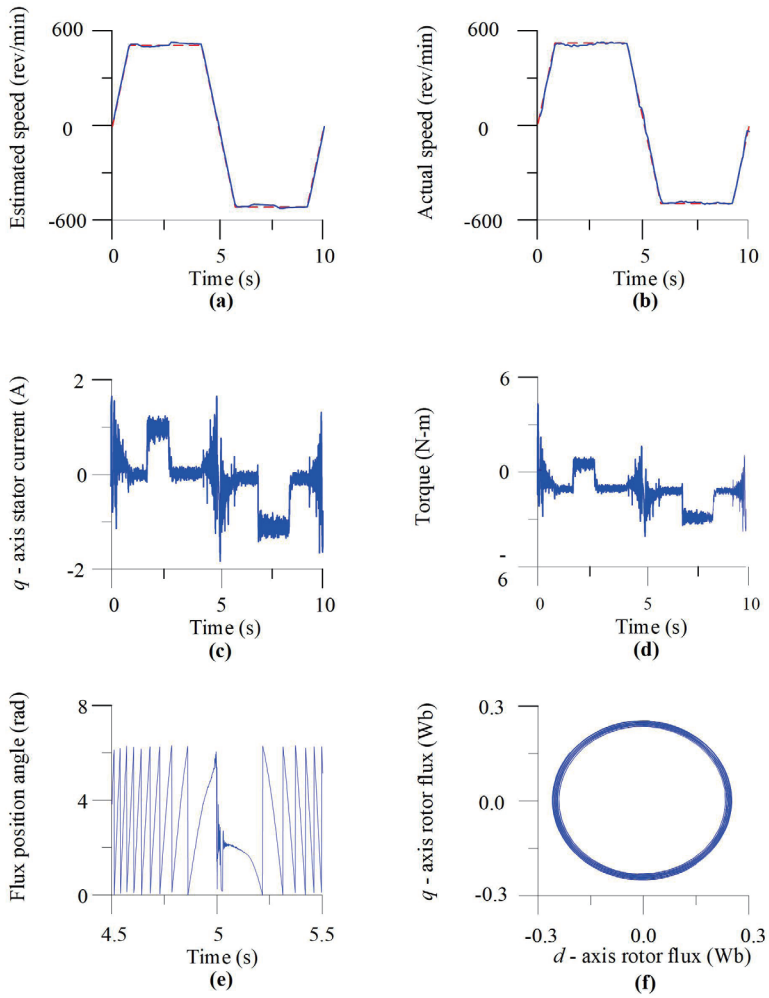

Fig. 6. (Color online) Experimental responses of the proposed FVC IPMSM drive using the flux observer speed estimation with a 2 N-m load for a reversible steady-state speed command of 500 rev/min: (a) estimated rotor speed, (b) actual rotor speed, (c) q-axis stator current, (d) electromagnetic torque, (e) flux position angle, and (f) rotor flux locus.

6. Conclusions

A speed estimation scheme using the flux observer was developed for a FVC IPMSM drive. The decoupled FVC IPMSM drive was established using the current and voltage of the stator. Lyapunov stability theory was used to design the flux observer speed estimation scheme, and the observer gain matrix design was used in the ABC algorithm. The three-phase stator currents for implementing the FVC IPMSM drive using the flux observer speed estimation scheme were provided by the Hall effect current sensors. Simulation and experimental results for reversible steady-state speed commands under a load condition confirmed the promising performance of the proposed FVC IPMSM drive using the flux observer speed estimation.

References

1 C. Wu, Z. Chen, and Q. Chen: IEEE Trans. Ind. Electron. **69** (2022) 1389. https://doi.org/10.1109/TIE.2021.3060676
2 E. Al-nabi, B. Wu, N. R. Zargari, and V. Sood: IEEE Trans. Ind. Electron. **60** (2013) 1711. https://doi.org/10.1109/TIE.2012.2191752
3 Q. Song, Z. Wang, P. Liu, Y. Xu, C. Tang, and M. Cheng: Proc. 2019 22th Int. Electrical Machines Systems Conf. (ICEMS, 2019) 1–5. https://doi.org/10.1109/ICEMS.2019.8921573
4 M. S. Basar, M. M. Bech, T. O. Andersen, P. Scavenius, and T. T. Basar: Proc. 4th Int. Power Engineering Energy Electrical Drives Conf. (ICPEED, 2013) 864–869. https://doi.org/10.1109/PowerEng.2013.6635723
5 A. Accetta, M. Cirrincione, M. Pucci, and G. Vitale: Proc. 2009 IEEE Int. Electric Machines Drives Conf. (IEMDC, 2009) 279–285. https://doi.org/10.1109/IEMDC.2009.5075218
6 J. Liu, T. A. Nondahl, J. Dai, S. Royak, and P. B. Schmidt: IEEE Trans. Ind. Appl. **56** (2020) 2180. https://doi.org/10.1109/TIA.2020.2977532
7 Z. Zhang: IEEE Trans. Pow. Electron. **37** (2022) 10290. https://doi.org/10.1109/TPEL.2022.3162963
8 L. Qu, W. Qiao, and L. Qu: IEEE Trans. Pow. Electron. **35** (2020) 6175. https://doi.org/10.1109/TPEL.2019.2953162
9 L. Qu, L. Qu, and W. Qiao: Proc. 2019 IEEE Energy Conversion Cong. Expo. (ECCE, 2019) 792–797. https://doi.org/10.1109/ECCE.2019.8913312
10 P. C. Biswas and B. C. Ghosh: Proc. 2017 3rd Int. Electrical Information Communication Technology Conf. (EICT, 2017) 1–6. https://doi.org/10.1109/EICT.2017.8275231
11 M. M. Gaballah, A. M. E. Nagar, E. A. G. E. Araby, M. E. Bardini, and M. M. Sharaf: Proc. 2021 Int. Electronic Engineering Conf. (ICEEM, 2021) 1–5. https://doi.org/10.1109/ICEEM52022.2021.9480380
12 N. V. Klinachev, N. Y. Kuleva, and S. G. Voronin: Proc. 2017 Int. Industrial Engineering Applications Manufacturing Conf. (ICIEAM, 2017) 1–4. https://doi.org/10.1109/ICIEAM.2017.8076390
13 Z. Novak and M. Novak: IEEE Trans. Power Electron. **37** (2022) 10154. https://doi.org/10.1109/TPEL.2022.3169708
14 K. K. Prabhakaran and A. Karthikeyan: IEEE Trans. Ind. Electro. **67** (2020) 5936. https://doi.org/10.1109/TIE.2020.2965499
15 M. M. Adel, W. A. Ahmed, M. Taha, and A. A. Saleh: Proc. 2020 Int. Power Electronics Electrical Drives Automation Motion Symp. (SPEEDAM, 2020) 5–10. https://doi.org/10.1109/SPEEDAM48782.2020.9161918
16 M. Nicola and C. I. Nicola: Proc. 2020 12th Int. Electronics Computers Artificial Intelligence Conf. (ECAI, 2020) 1–6. https://doi.org/10.1109/ECAI50035.2020.9223221
17 C. H. Liu: Control of AC Electrical Machines (Tunghua, Taipei, 2008) 4th ed., Chap. 6 (in Chinese).
18 N. Koshio, H. Kubota, I. Miki, and K. Matsuse: Proc. 2009 Int. Electrical Machines Systems Conf. (ICEMS, 2009) 1–5. https://doi.org/10.1109/ICEMS.2009.5382876
19 Y. C. Luo, X. H. Zheng, C. H. Liao, and Y. P. Kuo: Sens. Mater. **32** (2020) 1955. https://doi.org/10.18494/SAM.2020.2785
20 Y. Boutails, D. Theodoridis, T. Kottas, and M. A. Christodoulou: System Identification and Adaptive Control (Springer Verlag, Switzerland AG, 2014).
21 R. K. Jatoth and A. R. Rajasekhar: Proc. 2010 Int. Communication Control Computing Technologies Conf. (ICCCCT, 2010) 241–246. https://doi.org/10.1109/ICCCCT.2010.5670559